NeuroImage 223 (2020) 117362

Contents lists available at ScienceDirect

NeuroImage

journal homepage: www.elsevier.com/locate/neuroimage

The human corticocortical vestibular network

T.M. Raiser[a,b,1], V.L. Flanagin[a,b,1], M. Duering[b,c,e], A. van Ombergen[a,f], R.M. Ruehl[a,d], P. zu Eulenburg[a,b,g,*]

[a] German Center for Vertigo and Balance Disorders, University Hospital, Ludwig-Maximilians-University Munich, Germany
[b] Graduate School of Systemic Neurosciences, Munich, Germany
[c] Institute for Stroke and Dementia Research, University Hospital, Ludwig-Maximilians-University Munich, Germany
[d] Department of Neurology, University Hospital, Ludwig-Maximilians-University Munich, Munich, Germany
[e] Munich Cluster for Systems Neurology (SyNergy), Munich, Germany
[f] Department of Translational Neurosciences, Faculty of Medicine and Health Sciences, University of Antwerp, Antwerp, Belgium
[g] Institute for Neuroradiology, University Hospital, Ludwig-Maximilians-University Munich, Marchioninistrasse 15, 81377 Munich, Germany

ARTICLE INFO

Keywords:
Functional network
Structural network
Vestibular system
Comparative connectomics

ABSTRACT

Background: Little is known about the cortical organization of human vestibular information processing. Instead of a dedicated primary vestibular cortex, a distributed network of regions across the cortex respond to vestibular input. The aim of this study is to characterize the human corticocortical vestibular network and compare it to established results in non-human primates.

Methods: We collected high-resolution multi-shell diffusion-weighted (DWI) and state-of-the-art resting-state functional MR images of 29 right-handed normal subjects. Ten cortical vestibular regions per hemisphere were predefined from previous vestibular stimulation studies and applied as regions of interest. Four different structural corticocortical vestibular networks accounting for relevant constraints were investigated. The analyses included the investigation of common network measures and hemispheric differences for functional and structural connectivity patterns alike. In addition, the results of the structural vestibular network were compared to findings previously reported in non-human primates with respect to tracer injections (Guldin and Grusser, 1998).

Results: All structural networks independent of the applied constraints showed a recurring subdivision into identical three submodules. The structural human network was characterized by a predominantly intrahemispheric connectivity, whereas the functional pattern highlighted a strong connectivity for all homotopic nodes. A significant laterality preference towards the right hemisphere can be observed throughout the analyses: (1) with larger nodes, (2) stronger connectivity values structurally and functionally, and (3) a higher functional relevance. Similar connectivity patterns to non-human primate data were found in sensory and higher association cortices rather than premotor and motor areas.

Conclusion: Our analysis delineated a remarkably stable organization of cortical vestibular connectivity. Differences found between primate species may be attributed to phylogeny as well as methodological differences. With our work we solidified evidence for lateralization within the corticocortical vestibular network. Our results might explain why cortical lesions in humans do not lead to persistent vestibular symptoms. Redundant structural routing throughout the network and a high-degree functional connectivity may buffer the network and reestablish network integrity quickly in case of injury.

1. Introduction

With the evolution of methods like functional MRI and diffusion-weighted imaging, we are able to build a model of the connections within the human brain from a functional and structural point of view. The concept of a connectome was introduced by Sporns et al. (2005). In the past years it has become a research target to build a detailed human connectome for answering questions in neuroscience (Van Essen et al., 2013). Disease connectomics (Klauser et al., 2015) and comparative connectomics (e.g. Goulas et al., 2014; van den Heuvel et al., 2016) have gained attention for investigating differences and common substrates within and among species. In this study we aimed to comprehensively

* Corresponding author at: Institute for Neuroradiology, University Hospital, Ludwig-Maximilians-University Munich, Marchioninistrasse 15, 81377 Munich, Germany.
E-mail address: Peter.Zu.Eulenburg@med.uni-muenchen.de (P. zu Eulenburg).
[1] These authors indicates equal contribution.

https://doi.org/10.1016/j.neuroimage.2020.117362
Received 29 October 2019; Received in revised form 2 September 2020; Accepted 4 September 2020
Available online 9 September 2020

characterize the vestibular corticocortical structural and functional network of the human brain.

Besides whole brain connectomes, researchers work on subnetworks of several species on various scales. On a cellular level (microscale nm to μm; mesoscale μm to mm), retrograde tracers identify (long) interneuronal connections, usually in rodents and non-human primates. These invasive methods can also resolve directionality. On a macroscale level, diffusion weighted imaging is used as an indirect and non-invasive measurement of fiber orientations. This method is widely used for researching the human brain and cannot detect retrograde or anterograde directionality. Mapping the entire human brain on a cellular level in the living organism is a major technological challenges that is not (yet) realizable in comparison to other species (e.g. mouse connectome, Oh et al., 2014).

Different sensory networks have been characterized over the past years. In non-human primate research visual areas have been defined, connectomes and networks constructed and compared across species (Orban et al., 2004; Rosa and Tweedale, 2005; Wang et al., 2012). Auditory (Misic et al., 2018), pain (Kucyi and Davis, 2015), and olfactory (Milardi et al., 2017) networks have also been established.

Independent of the modality or methods used, it is essential to define the cortical areas of the specific (sensory) network or to choose an appropriate parcellation of the brain. In contrast to the auditory or visual system, where unimodal stimulation is feasible, and the system well characterized, manifold confounds have until recently hampered the definition of the human cortical vestibular system, in particular the multisensory nature of its inputs (Ruehl et al., 2017). Electrophysiological and retrograde tracer studies in the macaque have identified the primary vestibular cortical regions and their connectivity (Guldin and Grusser, 1998). Human homologue areas of these regions have also been identified (Lopez et al., 2012; zu Eulenburg et al., 2012; zu Eulenburg et al., 2013; zu Eulenburg et al., 2018b).

The vestibular system supplies us with information about head translation, rotation and orientation in a gravitational environment. Interestingly, contrary to other sensory modalities, central vestibular dysfunction is typically transient, and the respective brain regions, both cortical and subcortical, are thought to be responsible for these compensation mechanisms (Brandt et al., 1997). Interestingly, disorders or lesions of these central vestibular regions can cause vestibular deficits in the acute phase, but vertigo symptoms never persist in these patients (Brandt and Dieterich, 2017). This suggests a highly robust and redundant vestibular cortical network organization.

Hemispheric lateralization has been observed in several networks like language (Knecht et al., 2000) and the auditory system (Misic et al., 2018). Dieterich et al. (2003) also found a correlation with handedness and vestibular dominance of the ipsilateral hemisphere. Lesions in the right hemisphere seem to cause vestibular symptoms more often than lesions in the left hemisphere (Eguchi et al., 2019) and symptoms persist longer (e.g. Abe et al., 2012). Very recently it has been shown that functional lateralization of certain tasks or states correlates negatively with the corpus callosum probability of the connection (Karolis et al., 2019).

In our current study we aimed for a corticocortical vestibular network on a macroscale with non-invasive diffusion weighted imaging (DWI) and functional connectivity from high-quality multiband resting-state data. The human corticocortical vestibular network was to be compared to the tracer-based structural network in non-human primates (Guldin and Grusser, 1998). We analyzed the network with respect to its robustness, vulnerability and how this relates to the hubness of individual nodes as measured by degree and betweenness centrality. Last but not least a goal of this study was to investigate if there is a lateralization of the structural and/or functional vestibular corticocortical network and the role of commissural connections via the corpus callosum.

2. Materials and methods

We recruited 29 right-handed participants (age range: 20.5 - 36.7 years, mean age: 27.4 ± 4.3 years, 16 female), from a larger pool of participants (N~150) that did not have any history of a peripheral or central neuro-otological disease and showed normal vestibular function during a clinical head-impulse-test, Romberg stance, Babinski stepping and Babinski pointing tasks. All participants also had to exhibit a detectable torsional nystagmus in the video-oculography surveillance during galvanic vestibular stimulation for the functional localizer session of the study. All participants gave their written informed consent and were paid for participation. The local ethics committee of the Ludwig-Maximilians-Universität, Munich, approved the study in accordance with the latest revision of the Helsinki declaration from 2008.

The imaging data were acquired on a clinical 3T MRI scanner (SKYRA Siemens, Erlangen, Germany) with a 64-channel head/neck coil. During all scans, participants wore ear plugs and a dedicated head fixation device to limit head motion artifacts during structural and functional imaging (®Pearltec Crania adult, Schlieren, Switzerland).

A high-resolution T1-weighted image was acquired for each subject at the start of the study (TR= 2060 ms, TE= 2.17 ms, flip angle = 12 deg., FoV= 240mm, 320 × 320 matrix, 0.75mm isotropic voxel resolution, A-P phase encoding, GRAPPA 2). Multi-shell diffusion weighted images were obtained for three shells of (1)b= 1000 s/mm^2, (2)b= 1750 s/mm^2, and (3)b= 2500 s/mm^2 at a 1.75mm isotropic spatial resolution. Ten non-diffusion and 150 directions encoding scans were obtained with the following parameters: acquisition matrix 128 × 128, 72 slices, TR= 3800ms, TE= 104.8ms, FoV= 224 × 224 mm, slice thickness= 1.75 mm, multi-band factor 3 (Feinberg et al., 2010). Reverse phase encoding in a subsequent otherwise identical second run was applied to minimize susceptibility-induced distortions during post-processing.

Resting state fMRI images were obtained during which participants had their eyes open fixating a dot straight ahead. Here, eye movements were recorded (with the MRC camera built into MRI compatible binocular goggles; NordicNeuroLab, Bergen, Norway). The images (589 volumes) with whole-brain coverage (2.5mm isotropic resolution) were acquired in an interleaved slice order with multiband acceleration factor 6 (TR = 700 ms, TE = 33 ms, flip angle = 45 °, FoV = 210 mm, matrix size = 84 × 84, slice thickness 2.5mm, anterior-posterior phase encoding direction, prescan normalized). The resting-state scanning session contained 589 volumes at a TR of 0.7 s (total duration 6 minutes 52 seconds).

For a functional localizer of the vestibular regions, an additional fMRI with bimastoidal galvanic vestibular stimulation (GVS) was conducted. GVS was performed after topical anesthetic (Emla ® creme, AstraZeneca, Wedel, Germany; 5 g for each side, active substances: 25 mg Lidocain and 25 mg Prilocain) was applied to the skin of the mastoid bone and surrounding areas and left to soak for at least 45 minutes. Controlled by custom programs written in Matlab a 2.5mA sinusoidal stimulus with a frequency of 0.9Hz and duration of 10 seconds elicited naturalistic vestibular sway sensations fifteen times during this session. The MR images (500 volumes) with whole-brain coverage (2.5mm isotropic resolution) were acquired in an interleaved slice order with multiband acceleration factor 6 (TR = 700 ms, TE = 33 ms, flip angle = 45 °, FoV = 210 mm, matrix size = 84 × 84, slice thickness 2.5mm, anterior-posterior phase encoding direction).

Prior to data analysis, all data were entered into the MRI Quality Control tool (MRIQC, Version 0.10.3) (Esteban et al., 2017) to exclude any data sets with low quality data. Average framewise displacement (FD) and standardized DVARS were used as the main quality control measures for the functional sessions. Participants were excluded if any single average run FD value exceeded 0.6 mm, if more than 25 % of a participant's time points from one run were above 0.2 mm FD, or if the temporal derivative of the voxel time course variance (DVARS) re-

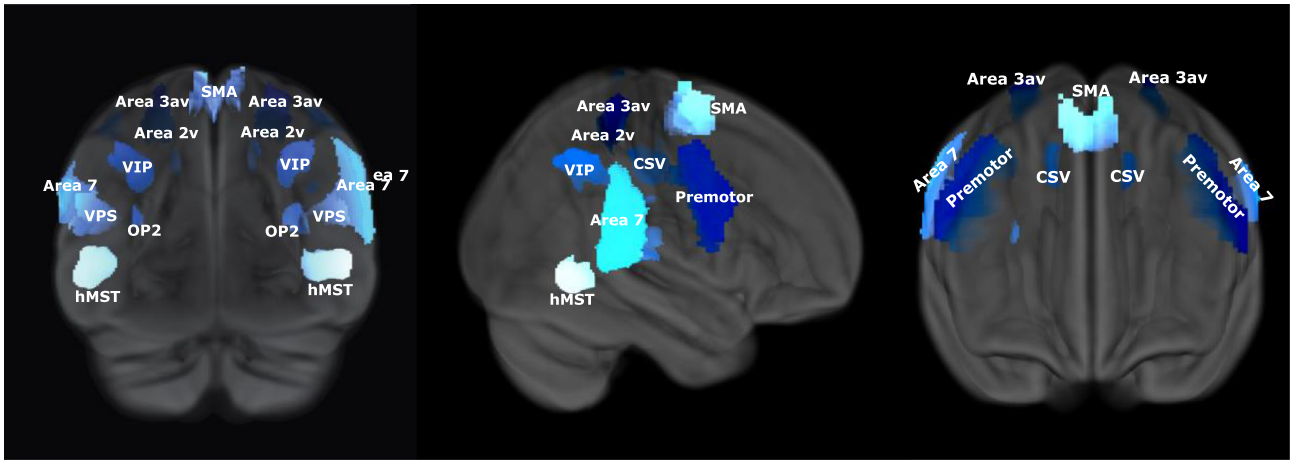

Fig. 1. Vestibular cortical regions. Bilaterally: Area 2v, Area 3av, Premotor, CSv, VIP, OP2, Area 7, VPS, SMA and hMST (in dorsal, right medial and frontal view).

flected more than 5% BOLD signal change (equivalent to a DVARS_nstd from MRIQC of over 50). None of the participants had to be excluded (see Supplemental 4 for the motion metrics from the resting-state fMRI data).

2.1. Vestibular Node definition

Defining robust, biologically motivated regions of interest is essential for an accurate connectome or network. In this study we targeted the vestibular cortical network. Ten cortical regions known in primates for vestibular processing were motivated from a large group study using whole-nerve galvanic vestibular stimulation for each hemisphere (zu Eulenburg et al., 2018a; zu Eulenburg et al., 2018b) (online at ScienceOpen.com DOI: 10.14293/S2199-1006.1.SOR-.PPCSDUO.v1) and used as regions-of-interest consisting of Area 2v, Area 3av, premotor area, cingulate sulcus visual (CSv), ventral intraparietal area (VIP), OP2, Area 7, visual posterior sylvian area (VPS), supplementary motor area (SMA) and human medial superior temporal area (hMST) (a detailed list of the nodes with size and coordinates can be found in Supplement 1). We chose this vestibular atlas, instead of a whole-brain parcellation such as the Schaefer atlas, because the dedicated vestibular regions often cover multiple parts of individual parcels, and at the same time belong to different networks, such as the salience network, the dorsal attention network and the somatomotor network (Supplemental 1,(Schaefer et al., 2018)).

For each subject we took the T1 to DWI co-registered image and created a deformation field (T1 to Montreal Neurological Institute (MNI) space) using the CAT12 toolbox (version: r1432; http://www.neuro.uni-jena.de/cat/index.html) in SPM12 (version: 7487). An inverse of the spatial deformation field was applied onto the atlas to generate an atlas on single subject level. We then created an intercept between a binarized grey matter mask (from the 5TT image; grey matter >0.1) and the atlas on single subject level to guarantee anatomical correctness with respect to tissue boundaries.

The vestibular atlas in MNI space is visualized in Fig. 1. The volume of the nodes varied across the established vestibular atlas. On average the right vestibular nodes were 23 % larger than the respective left nodes ($t(9)=2.27$, $p< 0.05$). (Fig. 2).

We compared this atlas with the subject's and the cohort's cortical response to galvanic vestibular stimulation (GVS). We calculated a similarity map for the group and for each single-subject response between the GVS activation pattern and the vestibular atlas and calculated the respective DICE overlap. The results can be found in Supplement 2. We also used the individual ROIs to calculate both the structural and functional vestibular network connectivity, and modularity (see Supplement 3), and found similar results to the atlas-based approach.

2.2. Structural connectivity analyses

2.2.1. Diffusion weighted data preprocessing and analysis

The DW images were visually inspected in all three orthogonal views and no severe artifacts were revealed, i.e. no signal dropout and no gross geometric distortions could be seen. Preprocessing was performed using MRtrix3 (http://www.mrtrix.org/; version: 3.0_rc3; Brain Research Institute, Melbourne, Australia), the FMRIB Software Library (FSL; Jenkinson et al., 2012), and Advanced normalization tools (ANTs; Avants et al., 2009). Preprocessing steps involved denoising (MRtrix 'dwidenoise'), Gibbs artefact removal (MRtrix 'mrdegibbs'), correcting for eddy currents, motion and susceptibility-induced distortions (FSL topup and eddy) and intensity bias corrections (ANTs 'N4biascorrection').

MRtrix3 was further used for constrained spherical-deconvolution (CSD) and anatomically-constrained whole brain probabilistic tractography (Tournier et al., 2007, 2012; Tournier et al., 2019). T1 images were registered to the DW images using ANTs (Avants et al., 2009). Segmentation was obtained through generating five-tissue-type (5TT) images (consisting of: grey matter, white matter, CSF, subcortical grey matter, lesions). In none of the participants lesions were detected through the segmentation. The anatomically informed response function was then estimated from the data using the dhollander option (Dhollander et al., 2016).

Fiber orientation distributions (FOD) were estimated from the data with a spherical deconvolution followed by a multi-tissue informed log-domain intensity normalization. With the anatomically-constrained tractography (ACT; Smith et al., 2012) ten million streamlines ($=10^7$ streamlines with a maximum length of 250 mm and a FOD amplitude cutoff of 0.06) were generated. The 5TT anatomical information in this step results in biologically greater accuracy (Smith et al., 2012). For visual inspection a subset of 10^5 streamlines was generated for each subject and overlaid on the 5TT images to check for correctness.

For the tractography we used gray and white matter interface cropped streamlines, the backtrack option and determined the seed points dynamically with the help of the white matter norm mask. ACT was used in combination with spherical deconvolution informed filtering of tractograms (SIFT2) to further improve the biological accuracy of streamlines (Smith et al., 2012, 2013, 2015).

2.2.2. Establishment of a structural corticocortical vestibular network (sCVN)

By means of combining the delineated 10 million streamlines and the above described vestibular atlas, we constructed corticocortical vestibular networks for each subject. Using the calculated weightings after SIFT2 filtering, we created symmetric, undirected structural connectiv-

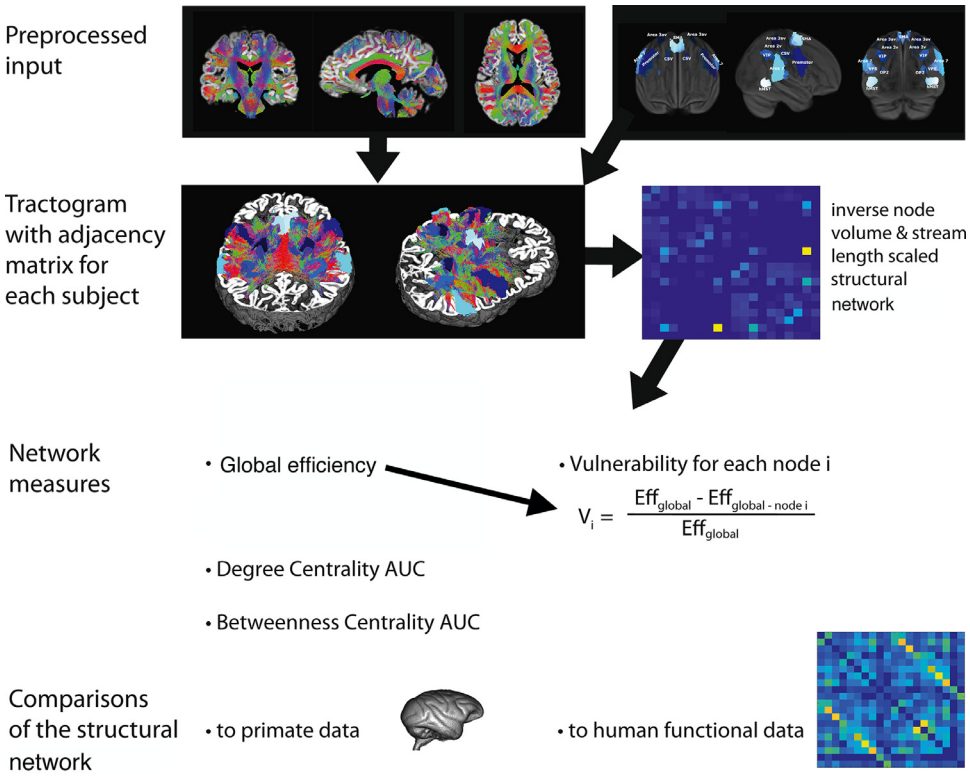

Fig. 2. Visualization of parts of the pipeline analyses. The tractogram as well as the adjacency matrices of the network were generated with MRtrix3 (detailed pipeline commands can be found in the supplement). Visualized is data of one representative subject. The functional data were generated with the CONN toolbox. The brain connectivity toolbox was used for generating network measures. AUC = Area under the curve.

ity matrices of all cerebral nodes with a diagonal set to zero. When not correcting for the distance between nodes, short-range connections are typically overestimated and local and global network statistics are not preserved (Betzel et al., 2019). We therefore scaled the weights by either inverse volume and/or inverse streamline length ((Hagmann et al., 2008)). This resulted in an unscaled version of the network as well as a streamline length scaled, an inverse node volume scaled and a scaled combined network. The focus of our analyses was the structural scaled combined network. The three additional structural networks were established to see whether the modularity of the network is stable across the differing constraints.

2.3. Establishment of a functional corticocortical vestibular network (fCVN)

A functional connectivity analyses was performed with the rsfMRI data using CONN toolbox (version 18b; Whitfield-Gabrieli and Nieto-Castanon, 2012; http://www.nitrc.org/projects/conn). Movement parameters, quality control timeseries and scrubbing regressors were employed by the CONN Toolbox as first level covariates. For denoising we used the following nuisance regressors' time series to lessen their impact: white matter (WM) and cerebrospinal fluid (CSF) confounds were considered with their first five principal components each. Furthermore, six principal temporal components of the movement parameters (three translation and three rotation parameters) as well as their six derivatives were employed. Images were denoised with a temporal band-pass filter (0.008-0.09 Hz). Scrubbing was selected as an option with default parameters to remove any images with higher motion, but no volumes in any participant were selected for scrubbing. The ROI-to-ROI analysis resulted in the functional weighted connectivity matrices with Fisher-transformed correlation coefficients. These results were thresholded at $p<0.05$ FDR corrected (two-sided) together with 1000 permutations for non-parametric thresholding in the CONN toolbox. This fCVN was used for detecting a stable number of modules within the network. For the subsequent network analyses, we set any negative correlation values to zero (Rubinov and Sporns, 2010, 2011). No further thresholds were applied to the functional network.

2.4. Brain connectivity analyses

2.4.1. Network modularity

The weighted undirected networks were all ordered by applying the community Louvain algorithm (Blondel et al., 2008) of the brain connectivity toolbox (BCT, version 2017-15-01; Rubinov and Sporns, 2010) iteratively onto the mean matrices of the four different scaled versions of the structural network as well as the functional network. With looping over several gamma values (ranging from 0 to 2.5) we detected a stable number of modules. The networks on single subject level were ordered accordingly. As we are not comparing two groups, we normalized the data for each subject to make the networks comparable to each other. The presence of a normal distribution of certain network measures was tested with the Anderson Darling test and then pairwise t-tests were performed to precisely test for significant differences between the right and the left hemispheres.

2.4.2. Network measures

In addition to the modularity, we were interested in network measures that reflect the resilience of nodes in the network, and how this relates to the hubness of the individual nodes. This is of particular importance for understanding the central vestibular compensation mechanisms after vestibular loss or dysfunction (Brandt and Dieterich, 2017). The following measures were only calculated for the structural network with stream length and inverse node volume scaled values, as well as the functional network: vulnerability, degree centrality and betweenness centrality.

To investigate the resilience of the network communication, we measured the vulnerability as described in Iturria-Medina et al. (2008). The vulnerability V_i was calculated for each node i by subtracting the global efficiency without node i from the global efficiency, and then dividing it by the global efficiency. The global efficiency was calculated for each node using the BCT. As vulnerability values can be both negative and

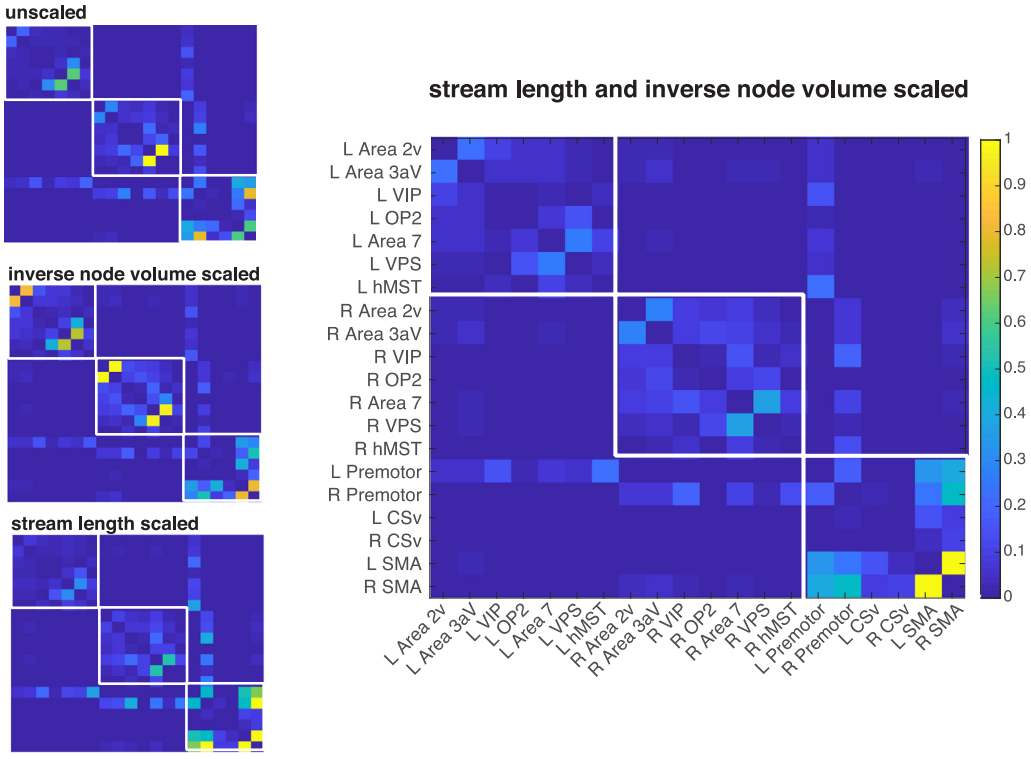

Fig. 3. Mean normalized structural matrices in community Louvain order: the unscaled, the inverse node volume scaled, and the stream length scaled network are listed on the left. The combined scaled network is shown bigger on the right. Higher values depict greater connectivity between regions. R corresponds to nodes in right hemisphere, L to the ones in the left hemisphere. Order of the node labels is identical for all four networks. White frames indicate stable modules assigned by the community Louvain algorithm.

positive and can change sign when applying different thresholds, we calculated the vulnerability for the adjacency matrices without thresholding them. Positive V_i values give rise to how important node i is for the global efficiency and removing node i harms the network efficiency. Negative values on the other hand indicate that the node is reducing the global efficiency. Values around 0 denote that the global efficiency does not change when node i is damaged or removed from the network.

To understand how the connectedness of individual nodes related to its vulnerability, we also calculated the degree centrality (DC) and betweenness centrality (BC), and can be combined with vulnerability. For every node we calculated the DC using the BCT after applying different thresholds onto the network, from 0 to 1 in 0.1 steps (corresponding to 0 to 0.76 correlation coefficients in the functional data). Putting thresholds on the matrices lowers the likelihood of false positive and false negative connections (de Reus and van den Heuvel, 2013). The area underneath the curve (AUC) of the degree centrality was calculated for each node with jackknife resampling of all subjects. To further investigate the homotopic organization of the brain, we performed a pair-wise t-test of the AUC values for left and right brain regions. For each node we further calculated the mean BC. For BC we calculated the AUC as described for DC.

2.5. Comparison with primate data

We compared our human structural scaled combined network to the connections reported in non-human primates of the homotopic vestibular ROIs. We took the mean values of the homotopic human nodes that led to a mean 10 × 10 structural network without hemispheric information. The connections between the analogous ROIs in primates, as defined in (Smith et al., 2017), were all generated via tracer projections (Guldin and Grusser, 1998), whereas our results originate from noninvasive imaging methods. Hence, we applied a filtering normalized threshold of 0.2 on our structural network to eliminate spurious connections. We considered connections with values between 0.6 and 1 as densely connected and values ranging from 0.2 to 0.6 as moderately dense connected. As we cannot detect directionality with our measures, we also extracted the non-human primate data without directionality from the literature. In non-human primates the connections were only reported as groups of either densely or moderately dense connected nodes (Guldin and Grusser, 1998). For the densely connected nodes, we chose a value of 0.8 and for the moderately dense connections a value of 0.4 for visualization purposes. Within the scope of the non-human primate tracer studies the majority but not all known cortical vestibular nodes have been investigated to date (e.g. periarcuate cortex, VIP) leaving us with eight out of ten nodes and its connections to compare descriptively. Area 3av was separated into Area 3aHv and Area 3aNV in the primate study but was combined to one region in our analysis.

3. Results

3.1. Characteristics of the structural CVN

A stable subdivision into three modules were generated consistently across all structural corticocortical vestibular networks (sCVN): (1) the left ROIs: Area 2v, 3av, IPS3, OP2, 7, VPS, hMST, (2) the right ROIs: Area 2v, 3av, IPS3, OP2, 7, VPS, hMST, and (3) bilaterally the premotor cortex, CSV and SMA (for the following gamma values: unscaled $0.59 \leq$ gamma ≤ 1.1; inverse node volume scaled $0.31 \leq$ gamma ≤ 0.9; stream length scaled $0.88 \leq$ gamma ≤ 1.05; combined $0.59 \leq$ gamma ≤ 1.1; Fig. 3). In all four networks the second module with right hemispheric nodes reveals higher intensities than the first module with the respective left hemispheric nodes. Hemispheric differences are addressed in a separate section below. Volume correction is obvious when comparing the inverse volume scaled network to the unscaled version. Connections between Area 2v and 3av gain weight as the nodes are relatively small in size and we corrected for the inverse of the node volume. Relatively

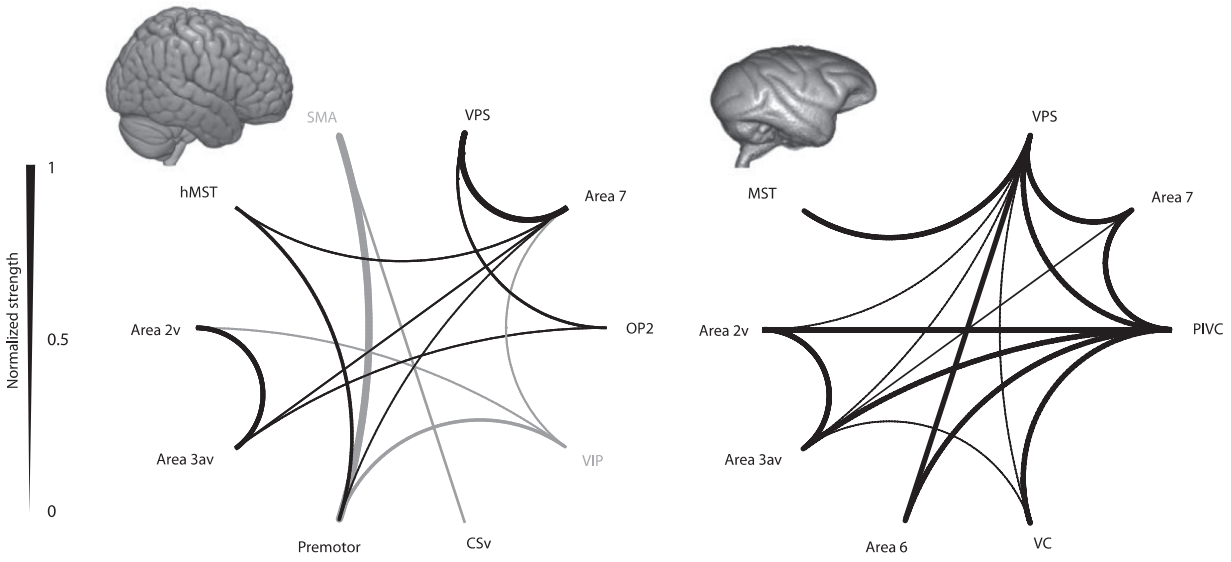

Fig. 4. Connectograms: (left) mean values across hemispheres of the normalized and weighted structural stream length and inverse node volume scaled network of humans with a threshold at 0.2, grey color indicates that a homologous region/connection was not taken into account in primates; human brain template in MNI space 3Drendered with MRIcroGL; (right) primate dense (thicker lines) and moderate dense (thinner lines) projections (right) between the respective homologous nodes reported by Guldin and Grusser (1998); image of the macaque brain was acquired from the INIA19 Primate Brain Atlas; brain pictures are not scaled according to their relative size.

large nodes' (e.g. premotor) connectivity values do not change drastically with inverse node volume correction. Further, the influence of correcting for the stream length is evident when comparing all four differently constrained networks. For example, Area VPS and Area 7 are in very close proximity in the brain and receive a highly dense connection attributed in those networks, which do not correct for stream length (i.e. unscaled and inverse node volume scaled). The same holds true for Area 2v and Area 3av. Stream length correction did not affect longer connections (e.g. Premotor – hMST) as much as shorter ones.

The premotor regions are overall densely connected within the according hemisphere and are highly connected with each other, as well as with the SMA of both hemispheres. Right and left SMA are densely interconnected and after correcting for stream length, SMA is ranked the most densely connected node of the network.

3.2. Homotopic organization of the network

Structurally we compared our results of the streamline strength and inverse node volume scaled network to connections reported in primates (Guldin and Grusser, 1998). We identified overlap and differences in connections between the vestibular nodes in human and non-human primates (Fig. 4). Unfortunately, we could not compare all connections of the vestibular nodes as two of the vestibular defined nodes (IPS3/VIP and periarcuate/SMA) were not reported in the tracer study of Guldin and Grusser (1998). On the one hand, we found some similarities between the two species in the vestibular structural networks. Two connections with very high density described in the human sCVN are also reported to be densely connected in primates: Area 2v – Area 3av, and VPS – Area 7. A rather moderately dense connection in humans of VPS and OP2 (0.33) is reported as a dense connection in primates (VPS-PIVC).

On the other hand, there is quite some difference in the reported connections. A moderate connection between hMST and the human premotor cortex (0.45), as well as hMST and Area 7 (0.23) are not reported in primates. A dense connection of MST and VPS in primates is not observable in the thresholded human connectogram. Further the densely connected PIVC in primates with several regions (VC, Area 6, Area 3av, Area 2v, VPS and Area 7) are mostly absent in the human equivalent OP2 (except a moderately dense connection to Area 3av (0.21) and to VPS (0.32)).

3.3. Hemispheric differences

We proceeded by comparing the left and right hemispheric node values of the human streamline strength and inverse node volume scaled network. The sum of the unthresholded intrahemispheric connections for each node was calculated for each hemisphere across subjects. The connectivity density values followed a normal distribution and were significantly larger for the right hemisphere compared to the left ($F(1,28) = 9.467$ $p = 0.0022$).

Repeated measures analyses of AUC DC and AUC BC for the inverse node volume and stream length scaled network showed significantly higher values for the right hemisphere ($F(1,28) = 3649.7$, $p \sim 0$, $F(1,28) = 194.2$, $p \sim 0$, respectively). The structural vulnerability was also higher for the right hemisphere ($F(1,28) = 11.069$, $p=0.000937$).

3.4. Network measures

Premotor and SMA areas are characterized by relatively high vulnerability values for the network (between 0.13 and 0.2) in comparison to the vulnerability values of the rest of the nodes that accumulate around 0 (Fig. 5). Even though the SMA (node 17 and 18) displays a lower AUC BC than the premotor areas (node 5 and 6), the vulnerability is comparably high (between 0.1 and 0.2). Premotor and SMA areas are characterized by a relatively high AUC DC in both hemispheres. The premotor areas are additionally characterized by a high AUC BC.

The remaining nodes cluster with relatively low centrality (AUC DC 0.75-1.5, AUC BC 1.5-6) and low vulnerability values around 0 and none of the nodes show lower values than -0.05 for the vulnerability.

3.5. Characteristics of the functional CVN

The functional network was divided into seven stable modules for $1.41 \leq \text{gamma} \leq 1.68$ with the iteratively performed community Louvain algorithm. Modules consist of bilateral (1) Area2v and Area 3aV, (2) Premotor Area, (3) CSv and VIP, (4) OP2, (5) Area 7, (6) VPS, and (7) SMA and hMST (Fig. 6).

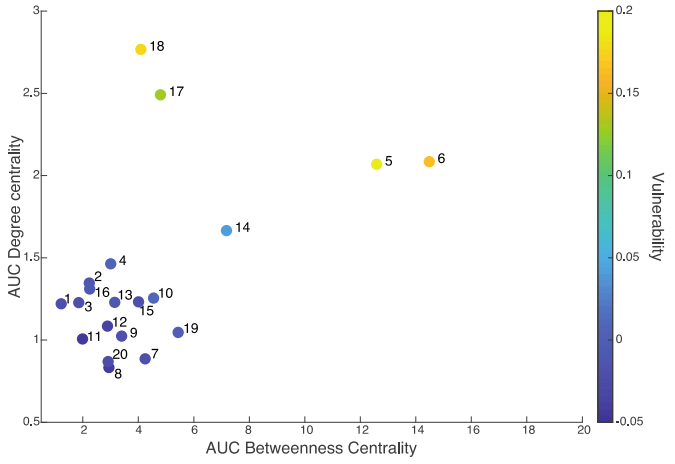

Fig. 5. Network measures for the stream length and inverse node volume scaled structural network. Color code visualizes the vulnerability of each node. Odd numbers are assigned to left hemispheric nodes, even numbers to right hemispheric nodes (1-2: Area 2v, 3-4: Area 3av, 5-6: Premotor, 7-8: CSv, 9-10: VIP, 11-12: OP2, 13-14: Area 7, 15-16: VPS, 17-18: SMA and 19-20: hMST).

No significant differences in the correlation coefficient between hemispheres was found. Investigating centrality measures a clustering of nodes is visible in the upper right corner of the graph (AUC DC between 3.9 and 5.9; AUC BC between 7.1 and 14.3). Both SMA regions (17 & 18) are spatially separated from this cluster with lower AUC DC and AUC BC values (see Fig. 6). For the functional network AUC DC and AUC BC did not show any hemispheric differences, however in general the higher the AUC DC and the higher the AUC BC, the higher the vulnerability of the nodes. Functional vulnerability was not significantly different between the two hemispheres. Right hemispheric areas VIP and VPS show the highest vulnerability in the functional network.

4. Discussion

The current results provide novel insights into the corticocortical organization of vestibular information processing in the human brain. We investigated the structural corticocortical vestibular network in humans across all established constraints (i.e. unscaled, streamline length scaled, inverse node volume scaled and a scaled combined network). We then compared the structural vestibular network with tracer-based findings in non-human primates (Guldin and Grusser, 1998). We discovered clear differences between the human and non-human primate

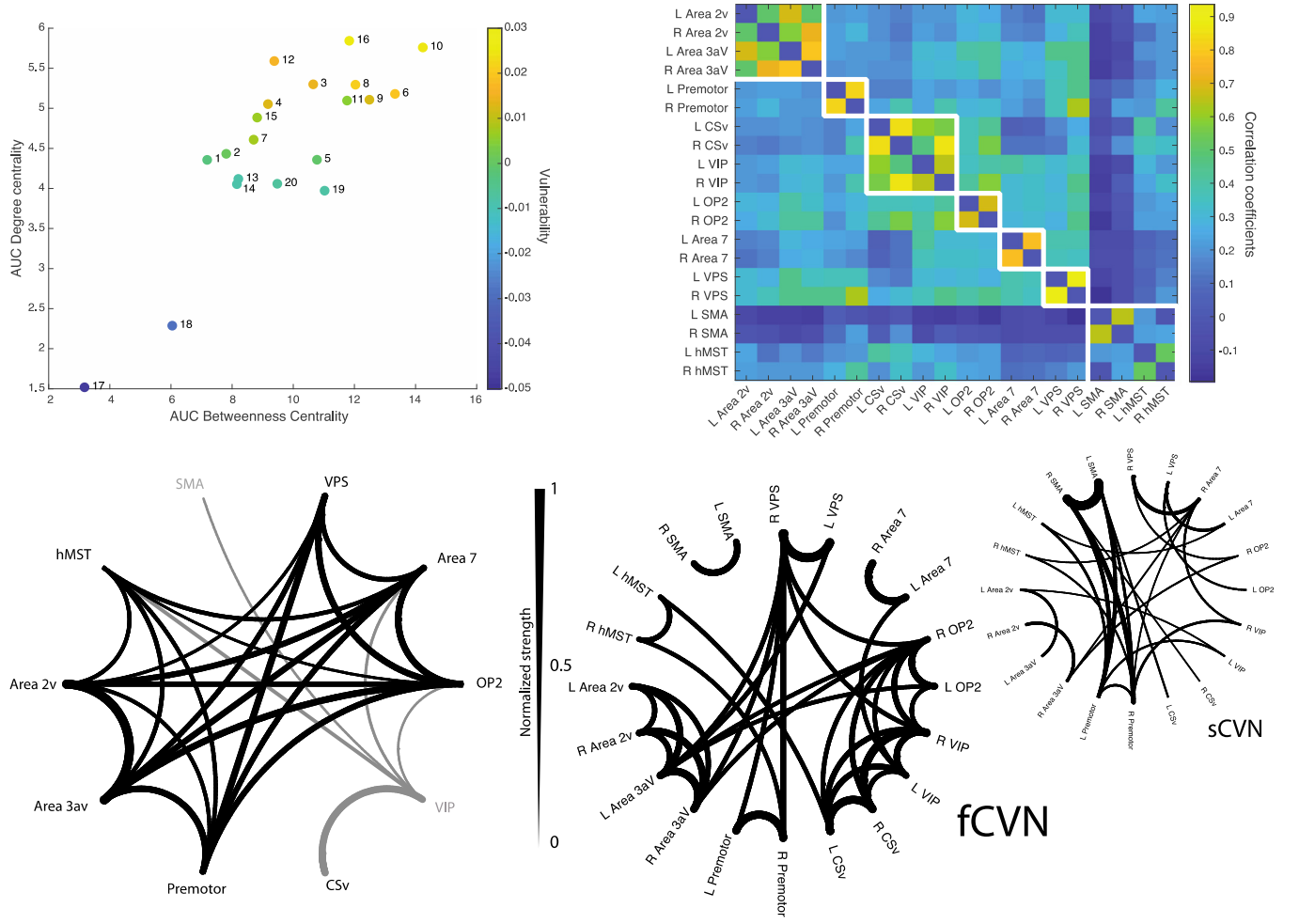

Fig. 6. (upper left) Network measures AUC Degree centrality, AUC betweenness centrality and vulnerability for all nodes of the functional network. Odd numbers are assigned to left hemispheric nodes, even numbers to right hemispheric nodes (1-2: Area 2v, 3-4: Area 3av, 5-6: Premotor, 7-8: CSv, 9-10: VIP, 11-12: OP2, 13-14: Area 7, 15-16: VPS, 17-18: SMA and 19-20: hMST); (upper right) Mean matrix of the functional community Louvain ordered network. Color of the matrix corresponds to the clustering coefficients between nodes. For further analyses negative values were set to zero. (lower left) Connectogram of the functional network thresholded at 0.2, grey color indicates that a homologous primate region/connection was not considered; (lower middle) connectogram of the fCVN with hemispheric information and a threshold at 0.4. For comparison reasons the sCVN connectogram with hemispheric information is shown on the lower right thresholded at 0.1. R corresponds to right hemisphere nodes, L to the left hemisphere nodes.

vestibular structural connections. The robustness of the vestibular network may explain why cerebral stroke patients with vertigo symptoms at onset never develop a chronic vestibular dysfunction.

4.1. Robust modularity of the cortical vestibular network across constraints

Independent of the constraints and scaling that were put on the structural networks, we consistently found three modules with identical composition. These modules were found irrespective of correcting or not correcting for stream length or node volume. These findings underpin the stability and robustness of the CVN network. Neither of the constraints resulted in a different separation of modules. The first two modules are homogenous for both hemispheres and may therefore be responsible for similar specialized processes. The third module of the structural CVN, consists of the premotor cortices, the SMA and CSv, and therefore represents general sensorimotor processing. These modules did not divide the vestibular regions into specific known functional networks, such as the somatomotor or dorsal attention network (Schaefer et al., 2018) but formed modules across networks.

4.2. The corticocortical vestibular network in human and non-human primates

We quantified the density of the connections between our predefined ROIs and compared them to previously reported connections in the macaque brain (Guldin and Grusser, 1998). Directly neighboring regions of interest are shown to be (densely) connected in both species (Area2v - Area3av, OP2/PIVC - VPS, VPS - Area7). The first two modules of the sCVN show similar connectivity to the macaque, suggesting a homology for the vestibular system between primate species.

We additionally found clear differences between the two species' networks. In the macaque brain, the PIVC is densely connected within the vestibular network. Dense structural connections of the human homologous OP2 region with other vestibular regions of interest are scarce. Functionally however, human area OP2 is very well interconnected with other vestibular regions. Indeed, the whole functional connectogram of humans shares more similarities with the macaques structural connectogram than the structural network of humans (but see following paragraph for potential limitations). However, even within the same species, a structural connection does not imply functional connectivity and vice versa. Consequently, interpretations and comparisons of structural and functional connectivity should be treated with caution.

While the clear differences between the structural networks of humans and macaques might be due to the investigation of two different species, they might as well arise due to the different methods used to obtain the structural networks. DWI-based tractography cannot detect the underlying anatomical connectivity on a micro scale and can only give us an estimation of the fiber orientation. In general, the interpretation of streamlines must be treated with caution: the resolution is too poor to detect the orientation of all fibers (Jones et al., 2013). With better resolution the chance of multiple orientations of fibers within one voxel decreases, but it will not reach the level of cellular organization. Conclusions about directionality cannot be drawn with DWI and graph theoretical methods (Klauser et al., 2015). Hence, at the moment, we lack the appropriate *in vivo* methods to quantify and compare connections from the human brain to other species. Tracer studies, although they have the cellular specificity, only a limited number of injections possible per animal and it is time-consuming work, and therefore all connections are typically not studied. Within our pool of regions two regions SMA and VIP were not reported in the macaques' network by Guldin and Grusser (1998). More work is needed to compare *in vivo* MRI and tracer injections within the same species across species to potentially overcome this obstacle as already pointed out by van den Heuvel et al. (2016). Limits of DWI in direct comparison with tracer injections are discussed elsewhere (Donahue et al., 2016; Reveley et al., 2015).

4.3. Structural vs. functional CVN

Our main goal of this work was to characterize the vestibular network itself without comparing it to other sensory subnetworks. Assuming DWI-based tractography provides an accurate assessment of the streamline fiber orientations, our combined structural and functional results suggest that the central vestibular information flow in humans works bottom-up through projection and association fibers without many structural commissural connections and information flow between the hemispheres. Structurally, we observed a robust intrahemispheric connectivity in most of the vestibular regions. Two modules consisting of seven brain regions were found in both hemispheres (Area 2v, 3av, IPS3, OP2, 7, VPS and hMST). Functionally however, all ten homotopic nodes of the left and the right hemisphere were strongly connected, despite the absence of structural connections (except premotor and SMA regions). Therefore, we hypothesize that vestibular information flow might spread bottom-up from either the brainstem or thalamic regions creating a high connectivity in the homotopic cortical nodes.

4.4. Cerebral laterality in the CVN

Our results suggest that the CVN has a right-sided dominance. Firstly, we observed this in the volume of the homotopic regions. Secondly, across all four structural networks, the connections were significantly stronger in the right hemisphere compared to the left. Karolis et al. (2019) recently investigated the functional lateralization in combination with structural corpus callosum connectivity across four different axes including communication, emotion, perception/action and decision. The vestibular network was not part of the laterality profile. Our results might help to close this gap: Within our vestibular network only two brain structures, premotor and SMA, were presented with interhemispheric connections via the corpus callosum and there seems to be a lateralization to the right. These results are in line with the reported results of Karolis et al. (2019) tested with other sensory modalities.

4.5. Remission of central vestibular symptoms due to cortical lesions

In about 5% of patients with dizziness, imbalance or vertigo symptoms an acute ischemic stroke is diagnosed (Kim et al., 2018). With lesions in one node or one connection of the vestibular network patients can suffer from vertigo in the acute stage prior and shortly after stroke (see review Brandt and Dieterich, 2017). Chronic central vestibular disorders however do not exist. That was the motivation for us to investigate the degree of vulnerability within the cortical vestibular network. Across our delineated networks we found characteristics, that might at least partly explain the generally transient nature of vestibular symptoms following a cerebral stroke. Hereto, the high degree of preexisting intrahemispheric structural connectivity might help to overcome lesion-associated symptoms occuring from stroke or other etiologies. In the acute state, functional connectivity might be reduced between homotopic regions leading to vertigo. But we infer from our results that depending on which edge or node is damaged, this information flow can be quickly rebuilt through an alternative route. The structural corticocortical network with the detected modules forms a good basis for this on a corticocortical level.

Our findings with respect to functional vulnerability being significantly higher in right hemispheric nodes are in line with previously reported higher prevalence of vestibular symptoms due to right hemispheric lesions (Eguchi et al., 2019). Further, Abe and colleagues reported longer rehabilitation time in the Pusher Syndrome (a disorder of postural balance that manifests as a pushing away toward the contralesional side in unilateral stroke) following right hemispheric lesions (2012). Whether there is a general difference in remission of vestibular symptoms depending on the lesion site needs to be further investigated

by comparing vulnerability profiles of the nodes with lesion mapping and vestibular symptom status.

4.6. Methodological considerations

We want to emphasize the quality of our generated dataset as we did not only include a reasonable number of subjects, but also guaranteed a state-of-the-art DWI data quality. DWI data quality benefitted from three shells (b-values of 1000, 1750 & 2500 s/mm^2) and 150 directions certainly improved the sensitivity of the fiber orientation (Jones et al., 2013). Previous studies of the vestibular system that have used single shell DWI data on bias-field prone scanners at lower resolutions than ours, make ambitious claims with regard to the corticothalamic or even brain stem-cortex connections within the vestibular network (e.g. Kirsch et al., 2016; Wirth et al., 2018). We fear that the investigators were neglecting limitations of the signal-quality of their data and the applied analytical methods. Because of this awareness of the profound limitations of DWI for deeper brain structures, we completely abstained from investigating any subcortical connectivity patterns. We also refrained from a whole-brain network analysis, and instead focussed specifically on the cortical vestibular brain regions because no whole-brain parcellation currently available represented the vestibular brain regions with the specificity and anatomical precision that our vestibular atlas does. We therefore focused this analysis on relative comparisons between different networks and between hemispheres.

Conclusion

With the present work, we described and characterized the cortico-cortical vestibular network. Modularity of the human structural corticocortical vestibular network is extremely robust. There is little overlap between the structural vestibular network in humans and monkeys. The human structural corticocortical vestibular network features a stronger intrahemispheric connectivity whereas the resting-state derived cortico-cortical vestibular network emphasizes a substantial functional connectivity of homotopic nodes. A laterality preference for the right hemisphere was observable in vestibular processing for the functional and structural analysis alike (stronger connectivity values, larger anatomical nodes, higher functional vulnerability in the right cerebral cortex).

There are obviously still many steps pending to fully understand the cortical vestibular organization and its embedding in and contribution to the whole-brain network. We are optimistic that our results and subsequent characterizations of the vestibular and adjacent subnetworks will further our understanding of the vestibular system in health and disease.

Declaration of Competing Interest

None.

Acknowledgement

We thank all participants for taking part in the experiment. Further, we thank Mathias Hübner for his technical MRI facility assistance, Judita Huber and Alex Knorr for methodological discussions and Judita Huber for calculating the overlap with the Schaefer400 atlas.

Funding

This work was supported by the Federal Ministry of Education and Research (BMBF 01 EO 0901) and a stipend of the Graduate School of Systemic Neurosciences grant DFG-GSC 82/3 (to TMR), a research fellowship (11U6414N and 11U6416N) and a research grant to stay abroad (V400717N) by the Research Foundation Flanders/FWO (to AVO), an Amelia Earhart fellowship by Zonta International (to AVO) and BELSPO Prodex (to AVO).

Supplementary materials

Supplementary material associated with this article can be found, in the online version, at doi:10.1016/j.neuroimage.2020.117362.

References

Abe, H., Kondo, T., Oouchida, Y., Suzukamo, Y., Fujiwara, S., Izumi, S., 2012. Prevalence and length of recovery of pusher syndrome based on cerebral hemispheric lesion side in patients with acute stroke. Stroke 43, 1654–1656.
Avants, B., Tustison, N., Song, G., 2009. Advanced normalization tools, ANTS 1.0. Sourceforge. Jun.
Betzel, R.F., Griffa, A., Hagmann, P., Mišić, B., 2019. Distance-dependent consensus thresholds for generating group-representative structural brain networks. Netw. Neurosci. 3, 475–496.
Blondel, V.D., Guillaume, J.-L., Lambiotte, R., Lefebvre, E., 2008. Fast unfolding of communities in large networks. J. Stat. Mech. Theory Exp. 2008, P10008.
Brandt, T., Dieterich, M., 2017. The dizzy patient: don't forget disorders of the central vestibular system. Nat. Rev. Neurol. 13, 352–362.
Brandt, T., Strupp, M., Arbusow, V., Dieringer, N., 1997. Plasticity of the vestibular system: central compensation and sensory substitution for vestibular deficits. Adv. Neurol. 73, 297–309.
de Reus, M.A., van den Heuvel, M.P., 2013. Estimating false positives and negatives in brain networks. Neuroimage 70, 402–409.
Dhollander, T., Raffelt, D., Connelly, A., 2016. Unsupervised 3-tissue response function estimation from single-shell or multi-shell diffusion MR data without a co-registered T1 image. ISMRM Workshop on Breaking the Barriers of Diffusion MRI.
Dieterich, M., Bense, S., Lutz, S., Drzezga, A., Stephan, T., Bartenstein, P., Brandt, T., 2003. Dominance for vestibular cortical function in the non-dominant hemisphere. Cereb. Cortex 13, 994–1007.
Donahue, C.J., Sotiropoulos, S.N., Jbabdi, S., Hernandez-Fernandez, M., Behrens, T.E., Dyrby, T.B., Coalson, T., Kennedy, H., Knoblauch, K., Van Essen, D.C., Glasser, M.F., 2016. Using diffusion tractography to predict cortical connection strength and distance: a quantitative comparison with tracers in the monkey. J. Neurosci. 36, 6758–6770.
Eguchi, S., Hirose, G., Miaki, M., 2019. Vestibular symptoms in acute hemispheric strokes. J. Neurol..
Esteban, O., Birman, D., Schaer, M., Koyejo, O.O., Poldrack, R.A., Gorgolewski, K.J., 2017. MRIQC: Advancing the automatic prediction of image quality in MRI from unseen sites. PLoS One 12, e0184661.
Feinberg, D.A., Moeller, S., Smith, S.M., Auerbach, E., Ramanna, S., Gunther, M., Glasser, M.F., Miller, K.L., Ugurbil, K., Yacoub, E., 2010. Multiplexed echo planar imaging for sub-second whole brain FMRI and fast diffusion imaging. PLoS One 5, e15710.
Goulas, A., Bastiani, M., Bezgin, G., Uylings, H.B., Roebroeck, A., Stiers, P., 2014. Comparative analysis of the macroscale structural connectivity in the macaque and human brain. PLoS Comput. Biol. 10, e1003529.
Guldin, W.O., Grusser, O.J., 1998. Is there a vestibular cortex? Trends Neurosci. 21, 254–259.
Hagmann, P., Cammoun, L., Gigandet, X., Meuli, R., Honey, C.J., Wedeen, V.J., Sporns, O., 2008. Mapping the structural core of human cerebral cortex. PLoS Biol. 6, e159.
Iturria-Medina, Y., Sotero, R.C., Canales-Rodriguez, E.J., Aleman-Gomez, Y., Melie-Garcia, L., 2008. Studying the human brain anatomical network via diffusion-weighted MRI and graph theory. Neuroimage 40, 1064–1076.
Jenkinson, M., Beckmann, C.F., Behrens, T.E., Woolrich, M.W., Smith, S.M., 2012. Fsl. Neuroimage 62, 782–790.
Jones, D.K., Knosche, T.R., Turner, R., 2013. White matter integrity, fiber count, and other fallacies: the do's and don'ts of diffusion MRI. Neuroimage 73, 239–254.
Karolis, V.R., Corbetta, M., Thiebaut de Schotten, M., 2019. The architecture of functional lateralisation and its relationship to callosal connectivity in the human brain. Nat. Commun. 10, 1417.
Kim, Y., Faysel, M., Balucani, C., Yu, D., Gilles, N., Levine, S.R., 2018. Ischemic stroke predictors in patients presenting with dizziness, imbalance, and vertigo. J. Stroke Cerebrovasc. Dis. 27, 3419–3424.
Kirsch, V., Keeser, D., Hergenroeder, T., Erat, O., Ertl-Wagner, B., Brandt, T., Dieterich, M., 2016. Structural and functional connectivity mapping of the vestibular circuitry from human brainstem to cortex. Brain Struct. Funct. 221, 1291–1308.
Klauser, P., Whittle, S., Simmons, J.G., Byrne, M.L., Mundy, L.K., Patton, G.C., Fornito, A., Allen, N.B., 2015. Reduced frontal white matter volume in children with early onset of adrenarche. Psychoneuroendocrinology 52, 111–118.
Knecht, S., Deppe, M., Drager, B., Bobe, L., Lohmann, H., Ringelstein, E., Henningsen, H., 2000. Language lateralization in healthy right-handers. Brain 123 (Pt 1), 74–81.
Kucyi, A., Davis, K.D., 2015. The dynamic pain connectome. Trends Neurosci. 38, 86–95.
Lopez, C., Blanke, O., Mast, F.W., 2012. The human vestibular cortex revealed by coordinate-based activation likelihood estimation meta-analysis. Neuroscience 212, 159–179.
Milardi, D., Cacciola, A., Calamuneri, A., Ghilardi, M.F., Caminiti, F., Cascio, F., Andronaco, V., Anastasi, G., Mormina, E., Arrigo, A., Bruschetta, D., Quartarone, A., 2017. The olfactory system revealed: non-invasive mapping by using constrained spherical deconvolution tractography in healthy humans. Front. Neuroanat. 11, 32.
Misic, B., Betzel, R.F., Griffa, A., de Reus, M.A., He, Y., Zuo, X.N., van den Heuvel, M.P., Hagmann, P., Sporns, O., Zatorre, R.J., 2018. Network-based asymmetry of the human auditory system. Cereb. Cortex 28, 2655–2664.
Oh, S.W., Harris, J.A., Ng, L., Winslow, B., Cain, N., Mihalas, S., Wang, Q., Lau, C., Kuan, L., Henry, A.M., Mortrud, M.T., Ouellette, B., Nguyen, T.N., Sorensen, S.A., Slaughter-

beck, C.R., Wakeman, W., Li, Y., Feng, D., Ho, A., Nicholas, E., Hirokawa, K.E., Bohn, P., Joines, K.M., Peng, H., Hawrylycz, M.J., Phillips, J.W., Hohmann, J.G., Wohnoutka, P., Gerfen, C.R., Koch, C., Bernard, A., Dang, C., Jones, A.R., Zeng, H., 2014. A mesoscale connectome of the mouse brain. Nature 508, 207–214.

Orban, G.A., Van Essen, D., Vanduffel, W., 2004. Comparative mapping of higher visual areas in monkeys and humans. Trends Cogn. Sci. 8, 315–324.

Reveley, C., Seth, A.K., Pierpaoli, C., Silva, A.C., Yu, D., Saunders, R.C., Leopold, D.A., Ye, F.Q., 2015. Superficial white matter fiber systems impede detection of long-range cortical connections in diffusion MR tractography. Proc. Natl. Acad. Sci. U S A 112, E2820–E2828.

Rosa, M.G., Tweedale, R., 2005. Brain maps, great and small: lessons from comparative studies of primate visual cortical organization. Philos. Trans. R. Soc. Lond. B Biol Sci 360, 665–691.

Rubinov, M., Sporns, O., 2010. Complex network measures of brain connectivity: uses and interpretations. Neuroimage 52, 1059–1069.

Rubinov, M., Sporns, O., 2011. Weight-conserving characterization of complex functional brain networks. Neuroimage 56, 2068–2079.

Ruehl, R.M., Stephan, T., Dieterich, M., zu Eulenburg, P., 2017. Towards a human vestibular cortex – Manifold confounders hamper the delineation of vestibular responses in functional neuroimaging. Clin. Neurophysiol. 128, e331–e332.

Schaefer, A., Kong, R., Gordon, E.M., Laumann, T.O., Zuo, X.N., Holmes, A.J., Eickhoff, S.B., Yeo, B.T.T., 2018. Local-global parcellation of the human cerebral cortex from intrinsic functional connectivity MRI. Cereb. Cortex 28, 3095–3114.

Smith, A.T., Greenlee, M.W., DeAngelis, G.C., Angelaki, Dora E., 2017. Distributed visual–vestibular processing in the cerebral cortex of man and macaque. 30, 91.

Smith, R.E., Tournier, J.D., Calamante, F., Connelly, A., 2012. Anatomically-constrained tractography: improved diffusion MRI streamlines tractography through effective use of anatomical information. Neuroimage 62, 1924–1938.

Smith, R.E., Tournier, J.D., Calamante, F., Connelly, A., 2013. SIFT: spherical-deconvolution informed filtering of tractograms. Neuroimage 67, 298–312.

Smith, R.E., Tournier, J.D., Calamante, F., Connelly, A., 2015. SIFT2: enabling dense quantitative assessment of brain white matter connectivity using streamlines tractography. Neuroimage 119, 338–351.

Sporns, O., Tononi, G., Kotter, R., 2005. The human connectome: a structural description of the human brain. PLoS Comput. Biol. 1, e42.

Tournier, J.D., Calamante, F., Connelly, A., 2007. Robust determination of the fibre orientation distribution in diffusion MRI: non-negativity constrained super-resolved spherical deconvolution. Neuroimage 35, 1459–1472.

Tournier, J.D., Calamante, F., Connelly, A., 2012. MRtrix: diffusion tractography in crossing fiber regions. Int. J. Imaging Syst. Technol. 22, 53–66.

Tournier, J.D., Smith, R., Raffelt, D., Tabbara, R., Dhollander, T., Pietsch, M., Christiaens, D., Jeurissen, B., Yeh, C.H., Connelly, A., 2019. MRtrix3: A fast, flexible and open software framework for medical image processing and visualisation. Neuroimage, 116137.

van den Heuvel, M.P., Bullmore, E.T., Sporns, O., 2016. Comparative connectomics. Trends Cogn. Sci. 20, 345–361.

Van Essen, D.C., Smith, S.M., Barch, D.M., Behrens, T.E., Yacoub, E., Ugurbil, K., Consortium, W.U.-M.H., 2013. The WU-Minn human connectome project: an overview. Neuroimage 80, 62–79.

Wang, Q.X., Sporns, O., Burkhalter, A., 2012. Network analysis of corticocortical connections reveals ventral and dorsal processing streams in mouse visual cortex. J. Neurosci. 32, 4386–4399.

Whitfield-Gabrieli, S., Nieto-Castanon, A., 2012. Conn: a functional connectivity toolbox for correlated and anticorrelated brain networks. Brain Connect. 2, 125–141.

Wirth, A.M., Frank, S.M., Greenlee, M.W., Beer, A.L., 2018. White matter connectivity of the visual-vestibular cortex examined by diffusion-weighted imaging. Brain Connect. 8, 235–244.

zu Eulenburg, P., Caspers, S., Roski, C., Eickhoff, S.B., 2012. Meta-analytical definition and functional connectivity of the human vestibular cortex. Neuroimage 60, 162–169.

zu Eulenburg, P., Muller-Forell, W., Dieterich, M., 2013. On the recall of vestibular sensations. Brain Struct. Funct. 218, 255–267.

zu Eulenburg, P., Stephan, T., Dieterich, M., Ruehl, R.M., 2018a. The human vestibular cortex. OHBM 2018 Organization for Human Brain Mapping, Republic of Singapore.

zu Eulenburg, P., Stephan, T., Dieterich, M., Ruehl, R.M., 2018b. The Human Vestibular Cortex, 30th Bárány Society meeting, Uppsala, Sweden.